Chapter 2

Fluctuations in the emission intensity from a RAM : Crossover from the Gaussian to the Lévy statistics

2.1 Motivation

In the previous chapter, we discussed in some detail the extensive experimental and theoretical studies that exist in literature on RAMs and followed it by a description of Gaussian and Lévy statistics. Chapter 1, thus provides the requisite background for the work described in this Thesis. In this chapter, we discuss our experimental and theoretical studies on fluctuations in the intensity of emission from dye-scatterer RAMs, over different realizations of its randomness. These random realizations originate variously in our experiments. For example, there is randomness inherent in the diffusive motion of the photon through the RAM. More explicitly, the spontaneously emitted seed photon can be generated at any position and in any random direction, within the RAM. Thereafter, this photon undergoes many random multiple scatterings off the passive scatterers into the bulk active medium, thereby getting amplified between successive scattering events, before it finally exits the RAM. Each spontaneously emitted photon, thus, follows a different random path through the RAM. Further, the configuration of the scatterers that are suspended in the liquid dye

solution is also changing constantly due to Brownian motion. This configurational change occurs over time-scales smaller than the interval between successive pump pulses (shots) in our experiments, and thus each shot samples a different random realization of the RAM, giving rise to the "sample-to-sample" fluctuation. Normally, these intensity fluctuations exhibit Gaussian statistics where the individual intensity values exhibit small deviations from a well-defined mean (following the CLT). However, a striking feature of the emission from a RAM is its non-selfaveraging nature [1]. Thus, the emission intensity fluctuates randomly over the ensemble of different microscopic realizations of the disorder in macroscopically identical bulk samples, when the gain is sufficiently high or scattering strong. Indeed, we find, both experimentally and theoretically, that for a range of parameters of the RAM, the intensity fluctuations are non-Gaussian and, in fact, show Lévy statistics over the ensemble of its random realizations. In particular, we observed that the amplification is dominated by certain improbable events that are "larger than rare", which give the intensity statistics a Lévy-like fat tail.

In this chapter, we first analyze theoretically the emission intensity from the dye-scatterer RAMs as a function of the two prime parameters, the gain length l_g and the transport mean free path l_t. We show that the intensity statistics follows a power-law behaviour, which suggests that either Gaussian or Lévy statistics may be observed in the intensity fluctuations depending on the scattering and the gain parameters characterizing the system. We then describe our experiments on dye-scatterer systems which indeed show Lévy intensity fluctuations in the limit of high gain (l_g^{-1}) and strong scattering (l_t^{-1}). Notably, we tailor a crossover from the Gaussian to the Lévy statistics and demonstrate continuous tunability of the Lévy exponent. This, to the best of our knowledge, provides the first experimental realization of non-Gaussian, in particular, Lévy statistics in the optics of a RAM, and the analysis thereof. The chapter concludes with a physical reasoning of our observations.

Before we begin the discussion of our work, it is worth noting that the statistical fluctuations in the emitted intensity from a RAM are quite different from the inherent photon statistics that arises due to fluctuations in emission for a given complexion as a function of time [2]. Statistical fluctuations of transmission/conductance through passive random me-

dia have been well studied, where, for a macroscopic sample, the classical fluctuations are small relative to the wave mechanical (or quantum) fluctuations due to coherent interference effects. In the present case we are strictly within the regime of classical diffusion, that is, $l_t \gg \lambda$, the wavelength of light; the anomalously large fluctuations are due entirely to the amplification inherent to a RAM.

2.2 Theoretical analysis

We consider a weakly scattering (diffusive) RAM composed of point-like scatterers randomly dispersed in an amplifying continuum. We assume, for simplicity, a spherical RAM of radius 'a', illuminated uniformly by a short pump-pulse at time $t = 0$ which serves to invert the population. A spontaneously emitted (seed) photon diffuses with diffusion constant $D = cl_t/3$, (c is the speed of light in the medium) getting amplified as it propagates, with gain $g = e^{ct/l_g}$, and finally exiting at time $t = T$ (Fig. 2.1).

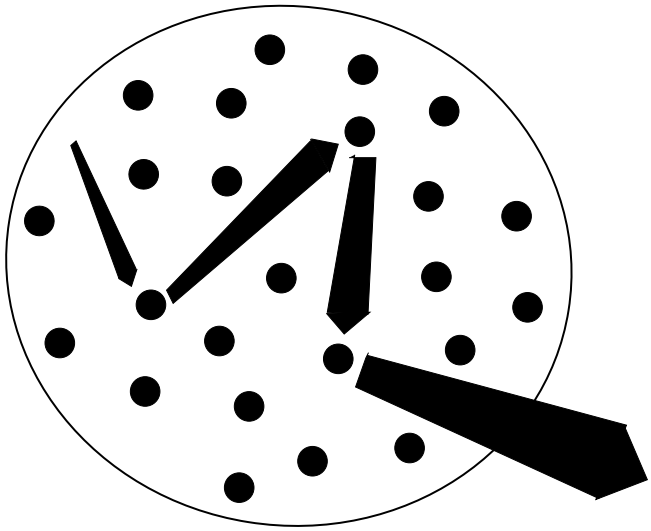

Figure 2.1: *Schematic of multiple scattering and amplification of a spontaneously emitted photon during its transit in the active bulk in between successive scattering events in a dye-scatterer RAM. (Line thickness is indicative of intensity)*

The rate of emission is, thus, the probability of escape of a photon from the surface ($r = a$) per unit time, with the photons spontaneously created at time $t = 0$ within the RAM at positions r, and is given by

$$p_I(t) = -\frac{\partial}{\partial t}\int_0^a \rho(\vec{\mathbf{r}}, t) d^3r = -\frac{\partial}{\partial t}\int_0^a \rho(\vec{\mathbf{r}}, t)\, 4\pi r^2 dr\ , \tag{2.1}$$

where, $\rho(\vec{\mathbf{r}}, t)$ is the probability density of the diffusing photon, emitted initially anywhere within the sample with a uniform initial probability density ρ_o. This requires the solution for the diffusion equation

$$\frac{\partial \rho(\vec{\mathbf{r}}, t)}{\partial t} = D\, \nabla^2 \rho(\vec{\mathbf{r}}, t) \tag{2.2}$$

Defining : $\tau = tD = t\ (cl_t/3)$, and separating variables as

$$\rho(\vec{\mathbf{r}}, \tau) = R(\vec{\mathbf{r}})\ T(\tau) \tag{2.3}$$

we obtain

$$\frac{\partial\ lnT(\tau)}{\partial \tau} = \frac{\nabla^2 R(\vec{\mathbf{r}})}{R(\vec{\mathbf{r}})} \quad = \quad -k^2 \tag{2.4}$$

which gives,

$$T(\tau) \quad = \quad e^{-k^2\tau} \tag{2.5}$$

$$\nabla^2\ R(\vec{\mathbf{r}}) \quad = \quad -k^2\ R(\vec{\mathbf{r}}) \tag{2.6}$$

The most general solution, in terms of spherical harmonics, is

$$R_k(r) \ = \ \sum_{l=0}^{\infty} C_{kl}\ Y_l(\theta, \phi)\ r^{-1/2}\ Z_{1/2}(kr) \tag{2.7}$$

where, $k = n\pi/a$, $n = 0, 1, 2, ...$

The initial condition is spherically symmetrical and so only $l = 0$ is retained. Thus,

$$R_k(r) \ = \ C_{k0}\ Y_0(\theta, \phi)\ r^{-1/2}\ Z_{1/2}(kr) \tag{2.8}$$

Using, $Y_0(\theta, \phi) = 1$ and $Z_{1/2}(kr) = \sqrt{2/\pi kr}\ sin(kr)$, we obtain

$$R_k(r) \ = \ C_{k0}\ \sqrt{\frac{2}{\pi k}}\ \frac{1}{r}\ sin(kr), \tag{2.9}$$

We get,

$$R_k(r = a) = 0 = C_{k0} \sqrt{\frac{2}{\pi k}} \frac{1}{r} sin(ka) \tag{2.10}$$

Substituting for k,

$$R_n(r) = C_{n0} \sqrt{\frac{2a}{n\pi^2}} \frac{1}{r} sin\left(\frac{n\pi r}{a}\right) \tag{2.11}$$

The coefficients C_n may be determined from the initial conditions as follows - using Eqs (2.3), (2.5) and (2.11), we get

$$\rho(\vec{\mathbf{r}}, \tau) = \sum_{n=1}^{\infty} C_{n0} \sqrt{\frac{2a}{n\pi^2}} \frac{1}{r} sin\left(\frac{n\pi r}{a}\right) e^{-(n\pi/a)^2 \tau} \tag{2.12}$$

Using the initial condition, $\rho(\vec{\mathbf{r}}, \tau = 0) =$ constant $= \rho_o$, we get

$$\rho_o = \sum_{n=1}^{\infty} C_n \sqrt{\frac{2a}{n\pi^2}} \frac{1}{r} sin\left(\frac{n\pi r}{a}\right) \tag{2.13}$$

Multiplying both sides of the Eq (2.13) by $sin(m\pi r/a)\, r$ and integrating, we have

$$\begin{aligned} \int_0^a \rho_o \, sin\left(\frac{m\pi r}{a}\right) r \, dr &= \sum_{n=1}^{\infty} C_n \sqrt{\frac{2a}{n\pi^2}} \int_0^a sin\left(\frac{n\pi r}{a}\right) sin\left(\frac{m\pi r}{a}\right) dr \\ &= \sum_{n=1}^{\infty} C_n \sqrt{\frac{2a}{n\pi^2}} \frac{a}{\pi} \int_0^{\pi} sin(nx)\, sin(mx)\, dx \\ &= C_m \sqrt{\frac{a^3}{2m\pi^2}} \end{aligned} \tag{2.14}$$

(using, $\pi r/a = x \Rightarrow dr = (a/\pi)\, dx$, and

$\int_0^{\pi} sin(nx)\, sin(mx)\, dx = 0 \quad : \; n \neq m$

$= \pi/2 \; : \; n = m$)

$$\begin{aligned} \Rightarrow \quad C_m &= \sqrt{\frac{2m\pi^2}{a^3}} \int_0^a \rho_o \, sin\left(\frac{m\pi r}{a}\right) r \, dr \\ &= \sqrt{\frac{2m\pi^2}{a^3}} \left(\frac{a}{\pi^2}\right)^2 \rho_o \int_0^{\pi} sin(mx)\, x \, dx \\ &= \sqrt{\frac{2a}{m}} \rho_o \, (-1)^{m+1} \quad : \; m = 1, 2, ... \end{aligned} \tag{2.15}$$

using Eqs (2.12), (2.13) and (2.15), we get

$$\rho(\vec{\mathbf{r}}, \tau) = \sum_{m=1}^{\infty} \left(\frac{2a\rho_o}{\pi m}\right) \frac{(-1)^{m+1}}{r} sin\left(\frac{\pi m r}{a}\right) e^{-(m\pi/a)^2 \tau} \tag{2.16}$$

In terms of t, we have

$$\rho(\vec{\mathbf{r}}, t) = \sum_{m=1}^{\infty} \left(\frac{2a\rho_o}{\pi m}\right) \frac{(-1)^{m+1}}{r} \sin\left(\frac{\pi m r}{a}\right) e^{-(m\pi/a)^2\ tD} \tag{2.17}$$

Substituting Eq (2.17) in Eq (2.1), we get

$$\begin{aligned} p_I(t) &= -\frac{\partial}{\partial t}\left[\sum_{m=1}^{\infty}\left(\frac{8a\rho_o}{m}\right)(-1)^{m+1} e^{-(m\pi/a)^2\ tD} \int_0^a \sin\left(\frac{\pi m r}{a}\right) r\, dr\right] \\ &= -\frac{\partial}{\partial t}\left[\sum_{m=1}^{\infty}\left(\frac{8a^3\rho_o}{m\,\pi^2}\right)(-1)^{m+1} e^{-(m\pi/a)^2\ tD} \int_0^{\pi} \sin(mx)\, x\, dx\right] \\ &= -\frac{\partial}{\partial t}\left[\sum_{m=1}^{\infty}\left(\frac{8a^3\rho_o}{m^2\,\pi}\right) e^{-(m\pi/a)^2\ tD}\right] \\ &= \sum_{m=1}^{\infty}(8\pi a\rho_o D)\, e^{-(m\pi/a)^2\ tD} \end{aligned} \tag{2.18}$$

$$\begin{aligned} &(using,\ \ \pi r/a = x \Rightarrow dr = (a/\pi)\, dx,\ \ and, \\ &\int_0^{\pi} \sin(mx)\, x\, dx = (-1)^{m+1}\frac{\pi}{m},\ \ \frac{\partial}{\partial t} e^{-(m\pi/a)^2\ tD} = -(m\pi/a)^2\ D\, e^{-(m\pi/a)^2\ tD}\ ) \end{aligned}$$

Now, the intensity gain is given as :

$$g = e^{ct/l_g} \tag{2.19}$$

$$\Rightarrow\ g \equiv g(t) \tag{2.20}$$

From the law of probabilities, we get

$$\begin{aligned} p_g(g)\, dg &= p_I(t)\, dt \\ \Rightarrow \qquad p_g(g) &= p_I(t)\, \frac{dt}{dg} \end{aligned} \tag{2.21}$$

Using Eqs (2.18), (2.19) and (2.21), we get

$$p_g(g) = \sum_{m=1}^{\infty}(8\pi a\rho_o D)\, \frac{l_g}{cg}\ e^{-m^2\pi^2 D l_g\ lng/a^2 c} \tag{2.22}$$

Thus,

$$p_g(g) = \sum_{m=1}^{\infty}(8\pi a\rho_o D)\, \frac{l_g}{cg}\ e^{ln\ g^{-\alpha_m}} = \sum_{m=1}^{\infty}(8\pi a\rho_o D)\, \frac{l_g}{cg}\, g^{-\alpha_m}, \tag{2.23}$$

where, $\alpha_m = (m\pi/a)^2\ D\, l_g/c = m^2(\pi^2 l_t l_g/3a^2)$

(using, $D = cl_t/3$ and $e^{ln\ (g)^{-\alpha m}} = g^{-\alpha_m}$)

The probability distribution for the gain $p_g(g)$ is thus obtained as

$$p_g(g) = \sum_{m=1}^{\infty} \left(\frac{8\pi a \rho_o D l_g}{c} \right) \frac{1}{g^{1+\alpha_m}} \equiv \sum_{m=1}^{\infty} \left(\frac{8\pi a \rho_o l_t l_g}{3} \right) \frac{1}{g^{1+\alpha_m}}, \tag{2.24}$$

where, $\alpha_m = m^2(\pi^2 l_t l_g / 3a^2) \equiv$ the mth Lévy exponent.

We now show that the smallest exponent α_1 dominates the sum, and it suffices to consider only the first term in Eq (2.24). From the expression (Eq 2.24) above, we get

$$ln\ (p_g(g)) = ln \left(\frac{8\pi a \rho_o l_t l_g}{3} \right) + ln \left(\sum_{m=1}^{\infty} g^{-(1+\alpha_m)} \right) \tag{2.25}$$

Considering only $m = 1$,

$$ln\ (p_g(g)) = ln \left(\frac{8\pi a \rho_o l_t l_g}{3} \right) - (1 + \alpha_1)\ ln\ g \tag{2.26}$$

with, $\alpha_1 = \pi^2 l_t l_g / 3a^2 \equiv$ the first Lévy exponent.

This is a straight line equation. $ln\ (p_g(g))$ depends linearly on $ln\ g$ with a negative slope $(1+\alpha_1)$. Figure 2.2 gives $p_g(g)$ as function of g (log-log scale), calculated from the expression (Eq 2.24) above by retaining increasing number of terms on the right-hand side for the RAM parameters : $l_g = 0.5$ cm, $l_t = 6 \times 10^{-4}$cm, $n_s = 10^{12}$/cc, $\rho_o = 0.5$/cc, $a = 1.0$ cm and $\lambda = 0.633$ μm. Interestingly, each of these appear as straight lines, and their slopes are seen to remain nearly the same indicating that $m = 1$ suffices for determining the Lévy exponent (α); the higher order terms serve to alter only the intercept. Thus,

$$p_g(g) \simeq \left(\frac{8\pi a \rho_o l_t l_g}{3} \right) \frac{1}{g^{1+\alpha_1}} \tag{2.27}$$

We now check for the normalization of $p_g(g)$ and calculate its first two moments.

Normalization :

$$\begin{aligned}
\int_{g=1}^{\infty} p_g(g) dg &= \frac{8\pi a \rho_o l_t l_g}{3} \sum_{m=1}^{\infty} \left(\int_{g=1}^{\infty} \frac{dg}{g^{1+\alpha_m}} \right) \\
&= \frac{8\pi a \rho_o l_t l_g}{3} \sum_{m=1}^{\infty} \frac{1}{\alpha_m} \\
&= \frac{8\pi a \rho_o l_t l_g}{3} \left(\frac{3a^2}{\pi^2 l_t l_g} \right) \sum_{m=1}^{\infty} \frac{1}{m^2} \\
&= \frac{4\pi a^3 \rho_o}{3} \qquad \left(using : \sum_{m=1}^{\infty} \frac{1}{m^2} = \frac{\pi^2}{6} \right)
\end{aligned} \tag{2.28}$$

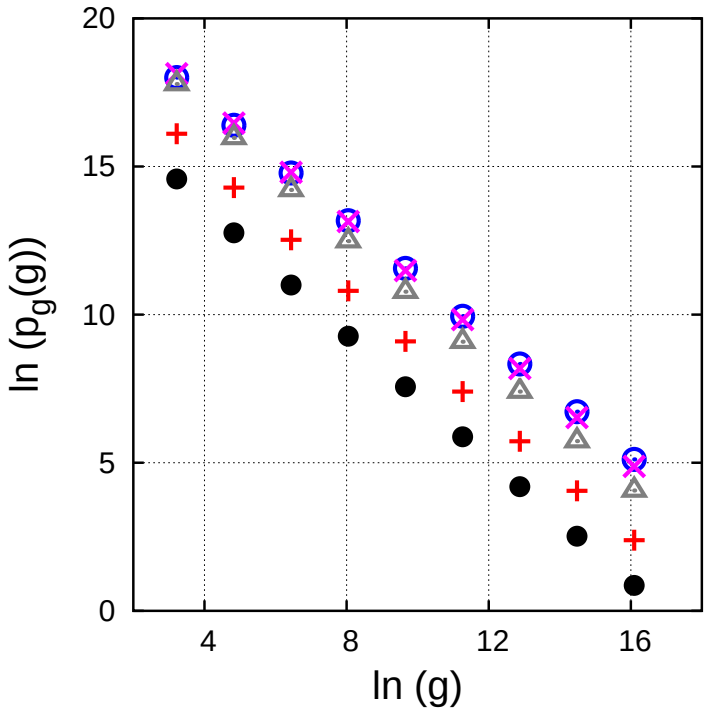

Figure 2.2: *Probability distribution of gain ($p_g(g)$) as function of gain (g), on a log-log scale, summed over different number of terms; ⊙ (blue) : m=1; × (pink) : m = 1 to 10; △ (gray) : m = 1 to 100; + (red) : m = 1 to 1000; • (black) : m=1 to 5000. The RAM parameters are : l_g = 0.5 cm, $l_t = 6\times10^{-4}$cm, $n_s = 10^{12}$/cc, ρ_o = 0.5/cc, a = 1.0 cm, λ = 0.633 μm.*

Thus, the normalization condition gives :

$$\begin{aligned} \int_{g=1}^{\infty} p_g(g)dg &= \frac{4\pi a^3 \rho_o}{3} = 1 \\ \Rightarrow \quad \rho_o &= \frac{1}{(4\pi a^3/3)} \ , \end{aligned} \tag{2.29}$$

where, $1/(4\pi a^3/3)$ is the volume of RAM of radius a.

First moment of g (mean value) :

$$\begin{aligned} < g > \ = \int_{g=1}^{\infty} g p_g(g)dg &= \frac{8\pi a \rho_o l_t l_g}{3} \sum_{m=1}^{\infty} \left(\int_{g=1}^{\infty} \frac{dg}{g^{\alpha_m}} \right) \\ &= \frac{8\pi a \rho_o l_t l_g}{3} \sum_{m=1}^{\infty} \left(\left| \frac{g^{1-\alpha_m}}{1-\alpha_m} \right|_1^{\infty} \right) \end{aligned} \tag{2.30}$$

Clearly, $< g >$ is finite for $\alpha_1 > 1$ i.e., for $l_g > 3a^2/\pi^2 l_t$. We then have,

$$< g > \; = \frac{8\pi a \rho_o l_t l_g}{3} \sum_{m=1}^{\infty} \left(\frac{1}{\alpha_m - 1} \right) \tag{2.31}$$

Thus, for high gain (low l_g) i.e., for $l_g < 3a^2/\pi^2 l_t$, the mean diverges.

Second moment of g :

$$\begin{aligned} < g^2 > \; = \int_{g=1}^{\infty} g^2 p_g(g) dg \; &= \frac{8\pi a \rho_o l_t l_g}{3} \sum_{m=1}^{\infty} \left(\int_{g=1}^{\infty} \frac{dg}{g^{\alpha_m - 1}} \right) \\ &= \frac{8\pi a \rho_o l_t l_g}{3} \sum_{m=1}^{\infty} \left(\left| \frac{g^{2-\alpha_m}}{2-\alpha_m} \right|_1^{\infty} \right) \end{aligned} \tag{2.32}$$

Clearly, $< g^2 >$ is finite for $\alpha_1 > 2$ i.e., for $l_g > 6a^2/\pi^2 l_t$. Then,

$$< g^2 > \; = \frac{8\pi a \rho_o l_t l_g}{3} \sum_{m=1}^{\infty} \left(\frac{1}{\alpha_m - 2} \right) \tag{2.33}$$

This corresponds to the Gaussian case. For high gain (low l_g) i.e., for $l_g < 6a^2/\pi^2 l_t$, the second moment diverges leading to divergent gain variance ($< g^2 > - < g >^2$). This is the Lévy case.

To summarize, for $0 < \alpha_1 < 2$, while the second moment of gain and hence, the gain variance always diverges, the mean gain may or may not exist (Lévy statistics). On the other hand, for $\alpha_1 \geq 2$, both the mean and the variance are finite (Gaussian statistics).

Clearly, $p_g(g)$ shows a power law behaviour. As discussed in chapter 1, this can describe either the Gaussian ($\alpha_1 \geq 2$) or the Lévy ($\alpha_1 < 2$) statistics. It is of interest to note that the condition for threshold of lasing i.e. *the divergence of mean gain* obtained by Letokhov [3] is

$$\frac{\pi^2 l_t l_g}{3a^2} = 1 \tag{2.34}$$

setting, $f = 1$ and $\alpha_{eff} = 1/l_g$ in Eq (22) of [3]. On the other hand, the condition for *divergence of variance of gain* as obtained by us is :

$$\frac{\pi^2 l_t l_g}{3a^2} = 2 \tag{2.35}$$

Thus, we can readily see that the divergence of the gain variance, that is the crossover from the Gaussian to the Lévy statistics will occur for a pumping level $(1/l_g)$ which is *lower* than that required for the divergence of mean gain (lasing threshold).

Evidently, with increasing pumping or increasing dye concentration, both of which serve to decrease l_g, the exponent α_1 decreases, the tail becomes fatter (rare events become more probable), and the variance of g diverges for $\alpha_1 < 2$. This suggests a means of controlling the crossover from a finite variance (Gaussian) to a divergent variance (Lévy) limit. Similar controlled crossover can also be achieved either by increasing the number density of scatterers or by enhancing the refractive index mismatch between the active bulk and the passive scatterers, both of which reduce l_t. Such tailoring of the exponent has been realized experimentally, and will be discussed shortly.

A few points may, however, be noted. The above analysis describes the onset of Lévy fluctuations as the gain (l_g^{-1}) or the scattering strength (l_t^{-1}) within the RAM is increased, idealized in that only the photons emitted spontaneously at time $t = 0$ were considered. These are amplified most anyway, and dominate the intensity, for large gains and scatterings. We have ignored the nonlinear effects like the temporal depletion of excited state population of the RAM by the amplification process itself. Further, for granular random media the grain size $\gg \lambda$, the random scattering is best described as random reflections/refractions at the interfaces. This can give rise to random closed loops that can trap and enhance light as in a resonance. Also, one can expect the classical Ruelle-Pollicott resonances giving pronounced structure to the fluctuation statistics. We have not addressed these finer issues here.

2.3 Experimental details

The emission from RAMs was studied by us in several dye-scatterer systems. In particular, we discuss the cases of Rhodamine 6G (R6G) and Rhodamine 640 (R640) perchlorate dyes (molar concentration : 5×10^{-3} M and 10^{-2} M) in ethanol with sub-micron (Titanium dioxide/rutile TiO_2 or polystyrene) microspheres randomly dispersed in them. The schematic of the experimental set-up is shown in Fig. 2.3. The RAM, contained in a glass cuvette of size

1 cm × 1 cm × 5 cm was pumped either by 10 ns pulse or 35 ps pulse at 532 nm from a frequency doubled Nd:YAG laser[1]. The incident pulse was split into two by a beamsplitter (R/T = 50/50). While the transmitted beam was focussed by a convex lens (f = 10 cm) to a spot of diameter ∼ 1.2 mm and was normally incident on the sample, the reflected part was used to monitor the energy of the pump pulse by the energy meter (Laser Probe Inc., Rj-7620). The pump energy was maintained constant throughout an experimental run. The emission (fluorescence) collected from the front face of the cuvette at an angle of 45^o to the direction of incidence was focussed by a convex lens (f = 10 cm) onto an optical fiber and the spectrum recorded on a PC based fiber-optic spectrometer (Ocean Optics S2000). To prevent coagulation of the scatterers, the suspension was shaken in an ultrasonic bath for ∼ 2 min before recording an emission spectrum. In order to obtain good statistics around five hundred single-shot spectra were recorded, for a given pump energy. The pulse-to-pulse fluctuations in emission intensity were then studied at a particular wavelength, for a wide range of parameters (namely, pump energy, dye concentration, scatterer density and type of scatterers) characterizing the RAM. It may be noted that the collected intensity (I_o) contains the unamplified spontaneous emission (I_{spont}) too, which must be subtracted, so as to ensure analysis of only the stimulated emission from the system. We will, in the rest of the chapter, refer to this intensity as $I = I_o - I_{spont}$. Intensity histograms were constructed for a chosen wavelength, by plotting the number of times an intensity value was obtained, normalized to the total number of spectra ($P(I)$), as function of the intensity (I).

2.4 Results

Gain narrowing

We first examined the emission intensity fluctuations for the dye-scatterer systems, optically pumped by 10 ns pulses (10 Hz repetition rate) from the frequency doubled (λ = 532 nm) Nd:YAG laser. It was ensured that gain narrowing occurred in the system. The TiO_2 and

[1]The experiments using picosecond pulses were carried out at National Centre for Ultrafast Processes (NCUFP), Chennai

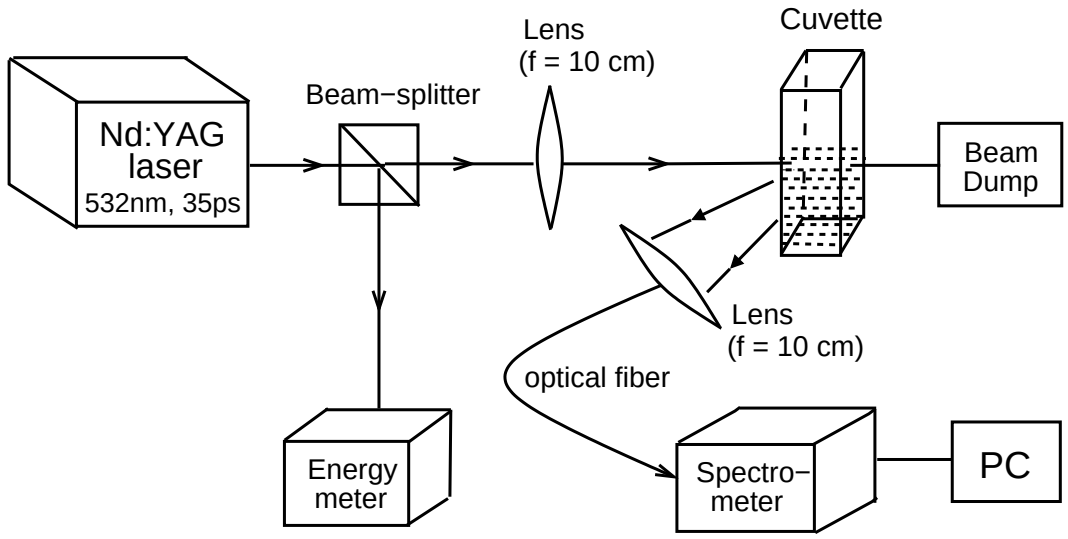

Figure 2.3: *Schematic of the experimental set-up.*

polystyrene microspheres used by us were of sizes (d) 0.36 μm and 0.30 μm respectively. Figures 2.4(a,c) show the emission spectra as function of pump energy for R6G(10^{-2} M)-TiO_2 and R640 perchlorate(10^{-2} M)-TiO_2 samples ($n_s = 2 \times 10^{10}$/cc) respectively. Each of the subfigure contains three spectra : (A), (B) and (C). Curves (A) give the emission spectra at low pumping, in fact, below the lasing threshold ($\sim$ a few tens of μJ). Clearly, the spectra are quite broad with full width at half maximum (FWHM) of $\sim$ 40 nm. On increasing the pump energy to just above the lasing threshold ($\sim$ 2 mJ), the FWHM drastically decreases to $\sim$ few nm (curves (B)). This corresponds to the onset of gain narrowing. The spectra have been scaled down by dividing them with a constant factor. Curves (C) represent the emission spectra much above the lasing threshold ($\sim$ 8 mJ). These too have been scaled down. Figures 2.4(b,d) give the intensity histograms for the same R6G(10^{-2} M)-TiO_2 and the R640 perchlorate(10^{-2} M)-TiO_2 systems respectively, at pump energy $\sim$ 8 mJ, well above the threshold for gain narrowing. Clearly, the statistics is Gaussian.

We expected that picosecond pumping would give different results. Firstly, a nanosecond pulse has a lesser peak intensity than that of a picosecond pulse of the same energy and focussed to the same spot-size. Further, the excited states of Rhodamine dyes have lifetime $\sim$ ns, and thus, during a 10 ns pulse, a significant number of molecules excited in the early part

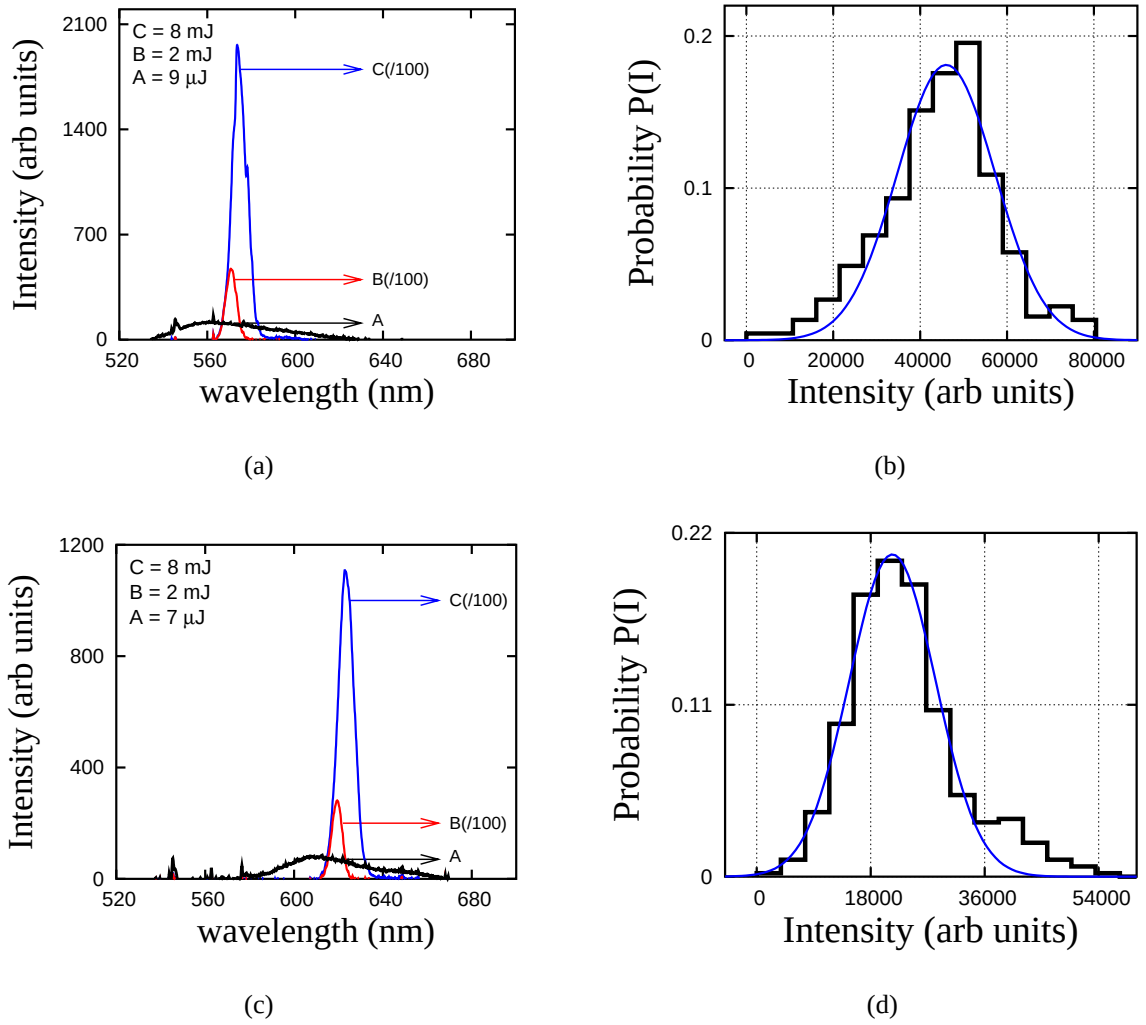

Figure 2.4: *Emission spectra as function of pump energy (nanosecond pulses) for, (a) R6G (10^{-2} M)-TiO_2, (c) R640 perchlorate (10^{-2} M)-TiO_2, (scatterer size = 0.36 µm, density = 2 × 10^{10}/cc). The corresponding intensity histograms and their Gaussian fits (blue curves) at pump energy ~ 8 mJ ; (b) and (d), respectively.*

of the pulse may have reverted to the ground state before the trailing edge of the pulse reaches the sample. Thus, high population inversion cannot be maintained. On the other hand, in the case of picosecond pumping, the upper state does not significantly decay spontaneously over the duration of the pulse. Thus, with picosecond pumping, lower gain length (l_g), may be achieved leading to enhanced amplification.

We, next, present the results with picosecond pulse pumping. Single-shot emission spectra as function of increasing pump energies from dye-scatterer systems with R6G dye and R640 perchlorate dye in ethanol containing TiO_2 or polystyrene microspheres as passive scatterers are shown in Figs 2.5 and 2.6 respectively. Table 2.1 gives the details of various RAMs studied for gain narrowing. Each subfigure (Figs 2.5(a)-(f)) and (Figs 2.6(a)-(d)) has three curves: (A), (B) and (C). Curves (A) represent the emission spectra obtained at lowest pumping ($\sim$ few tens of μJ) below the lasing threshold. Clearly, the emission spectra are quite broad with FWHM $\sim$ 30-40 nm. In fact, the spectra have to be multiplied by a factor to bring them to the same intensity scale as that of (B) and (C). Curves (B) are the emission spectra recorded on increasing the pump energy to above the gain-narrowing threshold ($\geq$ 40 μJ). The FWHM collapses to a $\sim$ a few nm. This can be attributed to higher gain within the RAM (which reduces the effective gain length) due to an increase in the pump energy. In most cases, (B) too have to be scaled up. Curves (C) correspond to the emission spectra recorded at pump energies much above the lasing threshold ($\geq$ 1 mJ). It is worth noting here that the nature of the spectra changes drastically; instead of a smooth peak with a width of few nanometers (as obtained with nanosecond pumping), several extremely narrow spikes ($<$ 1 nm) appear in the spectrum. This observation is consistent with the recent experimental reports [4, 5, 6] of spiked emission, which is interpreted as lasing. We shall shortly show, that in this regime the variance diverges and in some cases the mean too diverges, satisfying Letokhov's condition (Eq. (22) of [3]).

Intensity histograms

To recall, our aim in the present study is to examine the statistics of the pulse-to-pulse (equivalently, sample-to-sample) fluctuations in the emission intensity from the RAM over its dif-

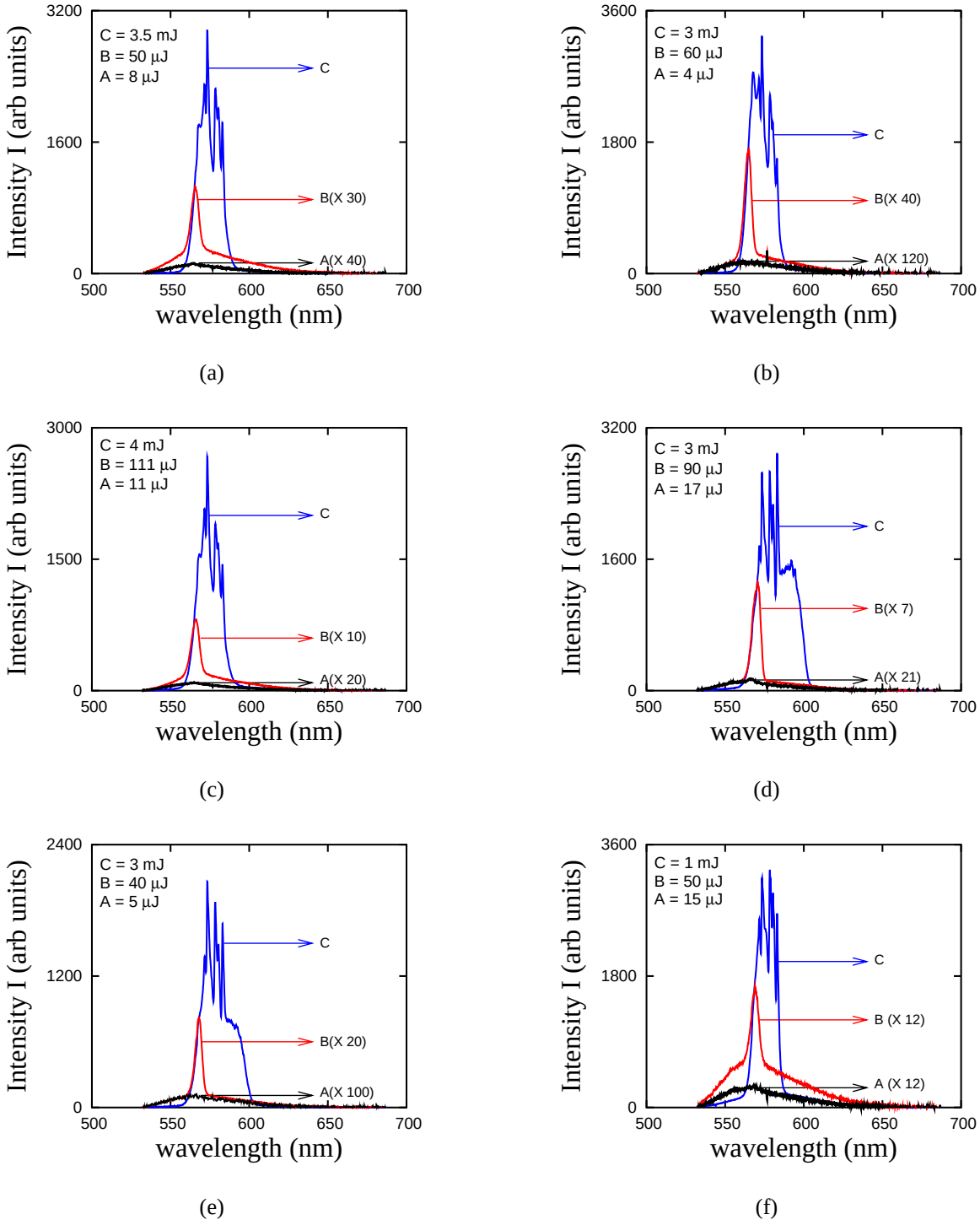

Figure 2.5: *Emission spectra as function of pump energy (picosecond pulses) for R6G (5 × 10^{-3}M) with, (a)TiO_2 (density = 10^{10}/cc), (b) TiO_2 (density = 2 × 10^{10}/cc), (c)polystyrene (density ~6.3 × 10^{11}/cc); and for R6G (10^{-2}M) with, (d)TiO_2 (density = 10^{10}/cc), (e)TiO_2 (density = 2 × 10^{10}/cc), (f)polystyrene (density ~6.3 × 10^{11}/cc). Polystyrene and TiO_2 microsphere sizes are 0.3 µm and 0.36 µm respectively.*

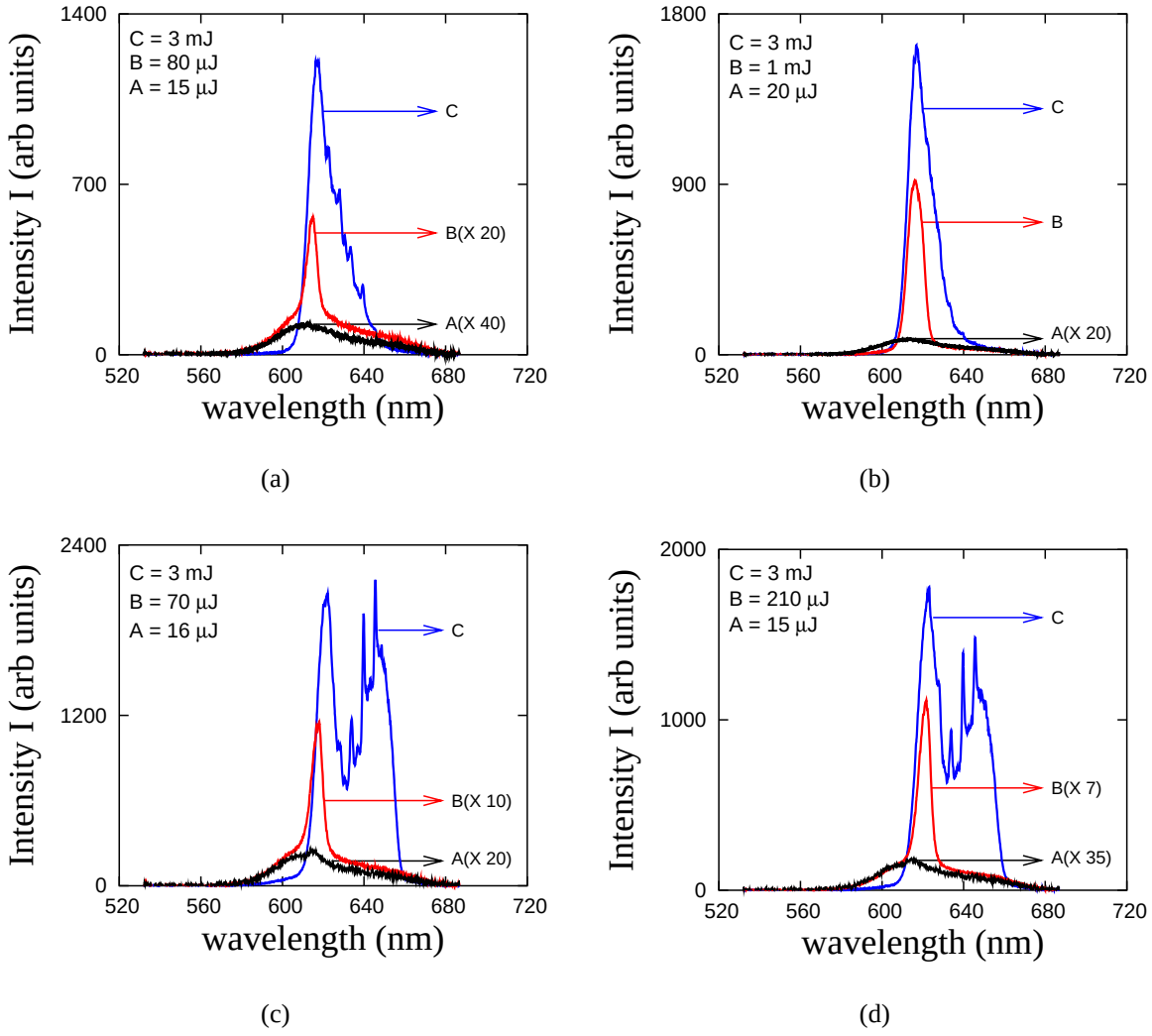

Figure 2.6: *Emission spectra as function of pump energy (picosecond pulses) for, (a) R640 perchlorate (5×10^{-3} M)-TiO_2 (density = 10^{10}/cc), (b) R640 perchlorate (5×10^{-3} M)-polystyrene (density ~6.3×10^{11}/cc), (c) R640 perchlorate (10^{-2} M)-TiO_2 (density = 10^{10}/cc), (d) R640 perchlorate (10^{-2} M)-polystyrene (density ~6.3×10^{11}/cc). Polystyrene and TiO_2 microsphere sizes are 0.3 µm and 0.36 µm respectively.*

S. No.	***Dye***	***Dye concentration*** (M)	***Scatterer***		
			type	***size*** (μ**m**)	***density*** (/**cc**)
1.	R6G	5×10^{-3}	TiO_2	0.36	10^{10}
2.	R6G	5×10^{-3}	TiO_2	0.36	2×10^{10}
3.	R6G	5×10^{-3}	polystyrene	0.30	6.3×10^{11}
4.	R6G	10^{-2}	TiO_2	0.36	10^{10}
5.	R6G	10^{-2}	TiO_2	0.36	2×10^{10}
6.	R6G	10^{-2}	polystyrene	0.30	6.3×10^{11}
7.	R640*	5×10^{-3}	TiO_2	0.36	10^{10}
8.	R640*	5×10^{-3}	polystyrene	0.30	6.3×10^{11}
9.	R640*	10^{-2}	TiO_2	0.36	10^{10}
10.	R640*	10^{-2}	polystyrene	0.30	6.3×10^{11}

Table 2.1: *Details of the samples studied for gain narrowing ($*$ ≡ perchlorate) with picosecond pulses.*

ferent random realizations. As we showed in section 2.2, from theoretical considerations, a controlled crossover from the finite variance (Gaussian) to the divergent variance (Lévy) limit is to be expected by altering the gain and scattering characteristics of the RAM. While, the gain can be varied by increasing the pumping or increasing dye concentration (decreasing l_g), the scattering strength can be varied by increasing the number density of scatterers or by enhancing the refractive index mismatch between the active bulk and the passive scatterers (decreasing l_t). Below we discuss all these cases for the different control parameters, characterizing the RAM, realized experimentally. Tables 2.2 and 2.3 give the details of the experimentally studied RAMs of which only a few representative cases have been discussed.

First, we present the results of our study on the statistical fluctuations of emission intensity from RAMs by altering the transport mean free path (l_t) via scatterer density. Figures 2.7(a,b,c) show the histograms for R6G (10^{-2} M) in ethanol with suspension of TiO_2 microspheres of size = 0.36 μm and densities $\sim 10^9/cc, \sim 10^{10}/cc$ and $\sim 2 \times 10^{10}/cc$ respectively, at pump energy of $\sim$ 3 mJ. Clearly, for low scatterer density ($\sim 10^9/cc$) the statistics

S. No.	***Dye concentration*** (M)	***Scatterer***			***Pump energy***
		type	***size*** (μ**m**)	***density*** (/**cc**)	
1.	5×10^{-3}	TiO_2	0.36	10^9	3 mJ
2.	5×10^{-3}	TiO_2	0.36	10^{10}	3 mJ
3.	5×10^{-3}	TiO_2	0.36	2×10^{10}	3 mJ
4.	5×10^{-3}	TiO_2	0.36	10^9	90 μJ
5.	5×10^{-3}	TiO_2	0.36	10^{10}	90 μJ
6.	5×10^{-3}	polystyrene	0.30	6.3×10^{11}	3 mJ
7.	5×10^{-3}	polystyrene	0.30	6.3×10^{11}	90 μJ
8.	5×10^{-3}	NIL	NIL	NIL	3 mJ
9.	10^{-2}	TiO_2	0.36	10^9	3 mJ
10.	10^{-2}	TiO_2	0.36	10^{10}	3 mJ
11.	10^{-2}	TiO_2	0.36	2×10^{10}	3 mJ
12.	10^{-2}	TiO_2	0.36	10^{10}	90 μJ
13.	10^{-2}	polystyrene	0.30	6.3×10^{11}	3 mJ
14.	10^{-2}	polystyrene	0.30	6.3×10^{11}	90 μJ
15.	10^{-2}	NIL	NIL	NIL	3 mJ

Table 2.2: *Details of R6G dye samples studied for observing the Gaussian-to-Lévy statistical crossover.*

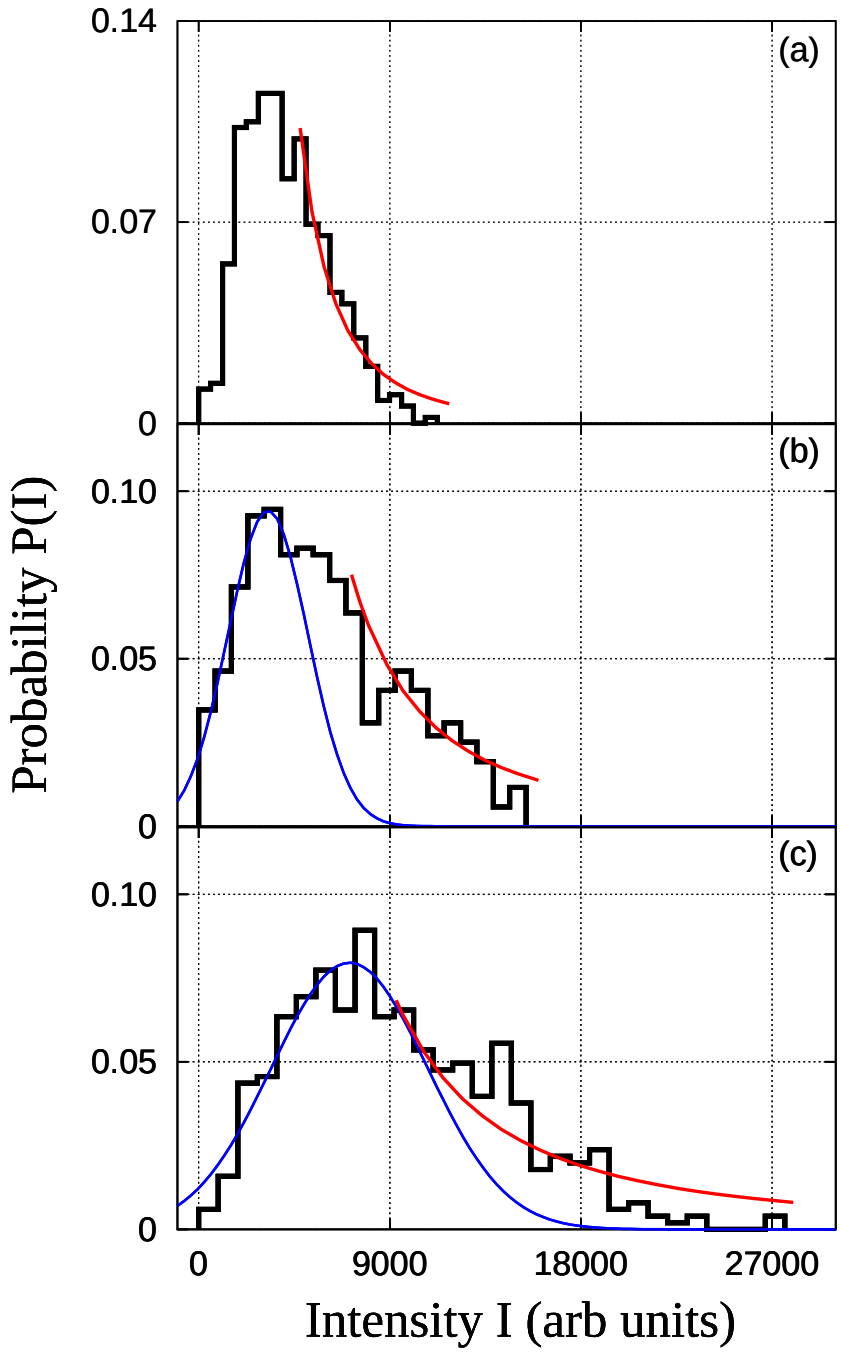

Figure 2.7: *Histograms for R6G(10^{-2} M)-TiO_2 system (pump energy ~ 3 mJ) for scatterer density (a) ~ 10^9/cc, (Gaussian) (b) ~ 10^{10}/cc, (Lévy,α = 1.13) (c) ~ 2×10^{10}/cc, (Lévy,α = 0.94). Blue and red curves show the Gaussian and the power-law fits, respectively, to the intensity histograms.*

S. No.	***Dye concentration*** (M)	***Scatterer***			***Pump energy***
		type	***size*** (μ**m**)	***density*** (/**cc**)	
1.	5×10^{-3}	TiO_2	0.36	10^{10}	3 mJ
2.	5×10^{-3}	polystyrene	0.30	6.3×10^{11}	3 mJ
3.	5×10^{-3}	NIL	NIL	NIL	3 mJ
4.	5×10^{-3}	TiO_2	0.36	10^{10}	90 μJ
5.	5×10^{-3}	polystyrene	0.30	6.3×10^{11}	90 μJ
6.	10^{-2}	TiO_2	0.36	10^{10}	3 mJ
7.	10^{-2}	polystyrene	0.30	6.3×10^{11}	3 mJ
8.	10^{-2}	NIL	NIL	NIL	3 mJ
9.	10^{-2}	TiO_2	0.36	10^{10}	90 μJ
10.	10^{-2}	polystyrene	0.30	6.3×10^{11}	90 μJ

Table 2.3: *Details of R640 perchlorate dye samples studied for observing the Gaussian-to-Lévy statistical crossover.*

is almost Gaussian (Fig. 2.7(a)). In fact, power-law fit ($g^{-(1+\alpha)}$) to the tail regime (large intensity values) of the intensity histogram yields the exponent $\alpha = 2$. As the scatterer density is increased to $\sim 10^{10}/cc$ (or l_t is decreased), a noticeable Lévy-like tail appears (Fig. 2.7(b)) implying a finite probability of occurrence of large intensity values. This, when fit to the power law function ($\sim g^{-(1+\alpha)}$) gives the Lévy exponent (α) of 1.13 (< 2). Thus, we could experimentally demonstrate crossover from the Gaussian ($\alpha = 2$) to the Lévy statistics ($\alpha = 1.13$) by increasing the scatterer density. On further increasing the scatterer concentration ($\sim 2 \times 10^{10}/cc$), the tail becomes quite pronounced (i.e., very large intensity values are observed), a power-law fit to which gives a Lévy exponent (α) of 0.94 (Fig. 2.7(c)). This, thus, demonstrates the tunability of the Lévy exponent (indicated by the decrease in α from 1.13 to 0.94).

We then studied the same R6G-TiO_2 system, as function of l_t (controlled via scatterer density), at a lower dye concentration of 5×10^{-3} M (which corresponds to lesser gain in the system). Figures 2.8(a,b) clearly show that the statistics is Gaussian at scatterer densities of

10^9/cc and 10^{10}/cc respectively. When the scatterer concentration is increased to 2×10^{10}/cc, a prominent Lévy tail is observed (Fig. 2.8(c)), a power-law fit to which gives the Lévy exponent (α) of 1.46 (< 2). On comparing Figures 2.7 and 2.8, we notice that the system characterized with a lower inherent gain (lesser dye concentration) requires larger scattering strength to exhibit the crossover to Lévy statistics.

Next, the scattering strength (l_t) was altered by varying the refractive index mismatch between the active bulk and the passive scatterers. Figures 2.9(a,b) show the histograms for R6G (10^{-2} M) in ethanol (pump energy $\sim$ 3 mJ) containing polystyrene microspheres (size = 0.30 μm, density $\sim 6.3 \times 10^{11}$/cc) and TiO_2 microspheres (size = 0.36 μm, density $\sim 2 \times 10^{10}$/cc), respectively. Clearly, while the R6G-polystyrene system exhibits Gaussian statistics, the R6G-TiO_2 system shows more pronounced Lévy features ($\alpha = 0.94 < 2$), despite it containing fewer scatterers. This is because, TiO_2 (refractive index $\sim$ 2.7) provides a higher refractive index mismatch with the surrounding solvent (ethanol, refractive index $\sim$ 1.36) as compared to polystyrene microspheres (refractive index $\sim$ 1.59). This results in increased scattering (smaller l_t) and hence, enhanced amplification.

Figures 2.10(a,b) show the intensity histograms for the same system studied at a lower dye concentration of 5×10^{-3} M. Though, the suspension of polystyrene microspheres result in Gaussian statistics, that of TiO_2 scatterers lead to Lévy statistics ($\alpha = 1.46$). It is worth noting here that the RAM characterized with a relatively lower gain (or lower dye concentration) exhibits Lévy statistics with a higher Lévy exponent (α) or less pronounced Lévy features.

Similar study was performed for a different dye. Figures 2.11(a,b) give the intensity histograms for R640 perchlorate dye (10^{-2} M) in ethanol with suspension of (a) polystyrene microspheres (size = 0.30 μm, density $\sim 6.3 \times 10^{11}$/cc) (b) TiO_2 scatterers (size = 0.36 μm, density $\sim 10^{10}$/cc). Clearly, while for R640 perchlorate-polystyrene sample the statistics is Gaussian, for R640 perchlorate-TiO_2 sample large intensity fluctuations result in Lévy statistics with an exponent (α) of 1.76 (< 2). Here, we notice that while the Gaussian-to-Lévy statistical crossover could be achieved both in the R6G and the R640 perchlorate dyes as function of refractive index mismatch, the Lévy feature is more pronounced (or α is

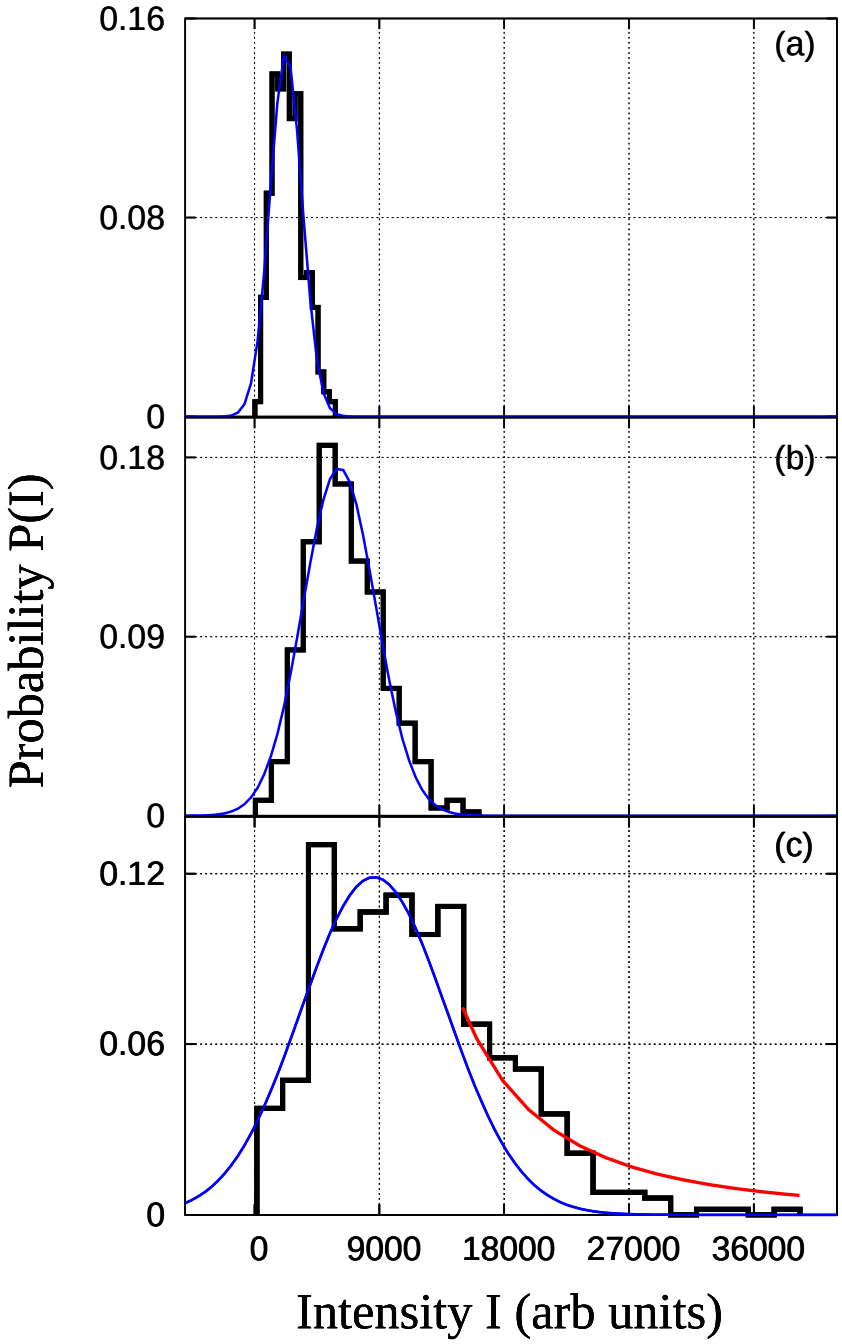

Figure 2.8: *Histograms for R6G (5×10^{-3} M)-TiO_2 system (pump energy ~ 3 mJ) for scatterer density (a) ~ 10^9/cc, (Gaussian) (b) ~ 10^{10}/cc, (Gaussian) (c) ~ 2×10^{10}/cc, (Lévy, $\alpha = 1.46$). Blue and red curves show the Gaussian and the power-law fits, respectively, to the intensity histograms.*

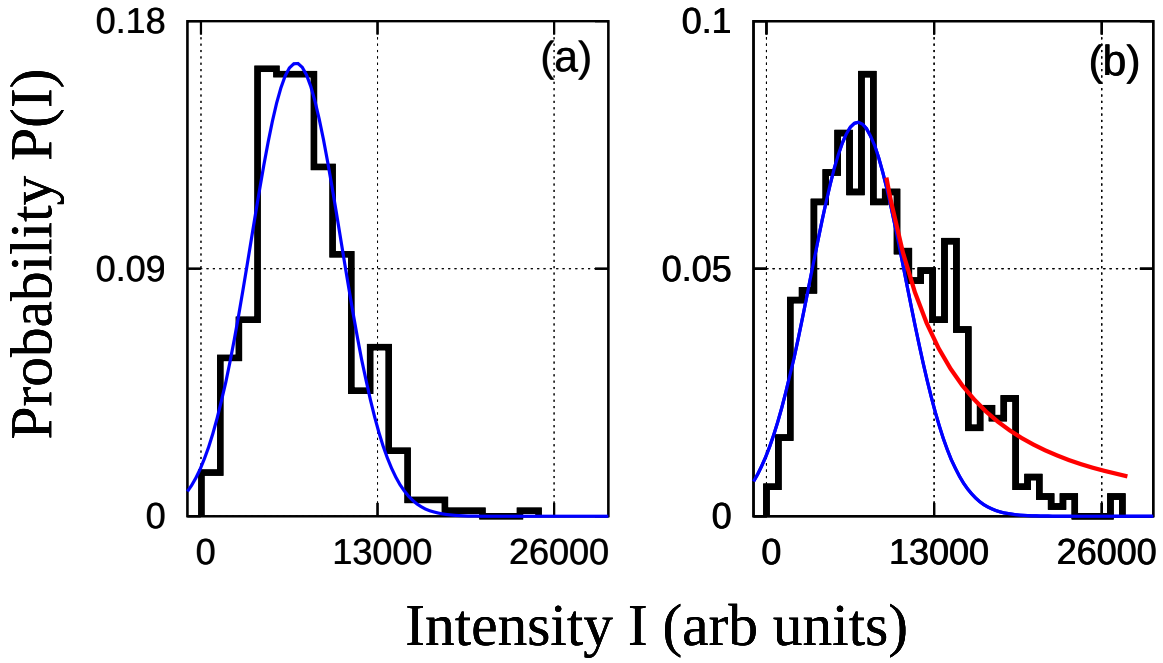

Figure 2.9: *Histograms for R6G (10^{-2} M) dye in ethanol (pump energy ~ 3 mJ) containing (a) polystyrene microspheres (size = 0.30 μm, density ~6.3 $\times$ 10^{11}/cc), showing Gaussian statistics (b) TiO_2 microspheres (size = 0.36 μm, density ~ 2 $\times$ 10^{10}/cc), showing Lévy statistics (α = 0.94). Blue and red curves show the Gaussian and the power-law fits, respectively, to the intensity histograms.*

smaller) in R6G than in R640 perchlorate suggesting that the R6G dye has a higher quantum efficiency than the R640 perchlorate dye.

Thus, the crossover from the Gaussian to the Lévy statistics has been experimentally demonstrated by two different means (namely, scatterer density and the refractive index mismatch), both of which alter the scattering strength (l_t) within the RAM.

Next, we examined the statistical fluctuations in emission intensity as function of gain (l_g^{-1}) in the RAM. First, we altered the gain length (l_g) by varying the pump energy. Figure 2.12(a) gives the histogram observed from R6G (10^{-2}M) in ethanol containing TiO_2 microspheres at sub-threshold pumping (~ 90 μJ), for which the emission has a spectral width of ~10 nm. The histogram is Gaussian. Figure 2.12(b) gives the histogram, when the pump energy was increased to 3 mJ (for which the corresponding emission spectra showed several

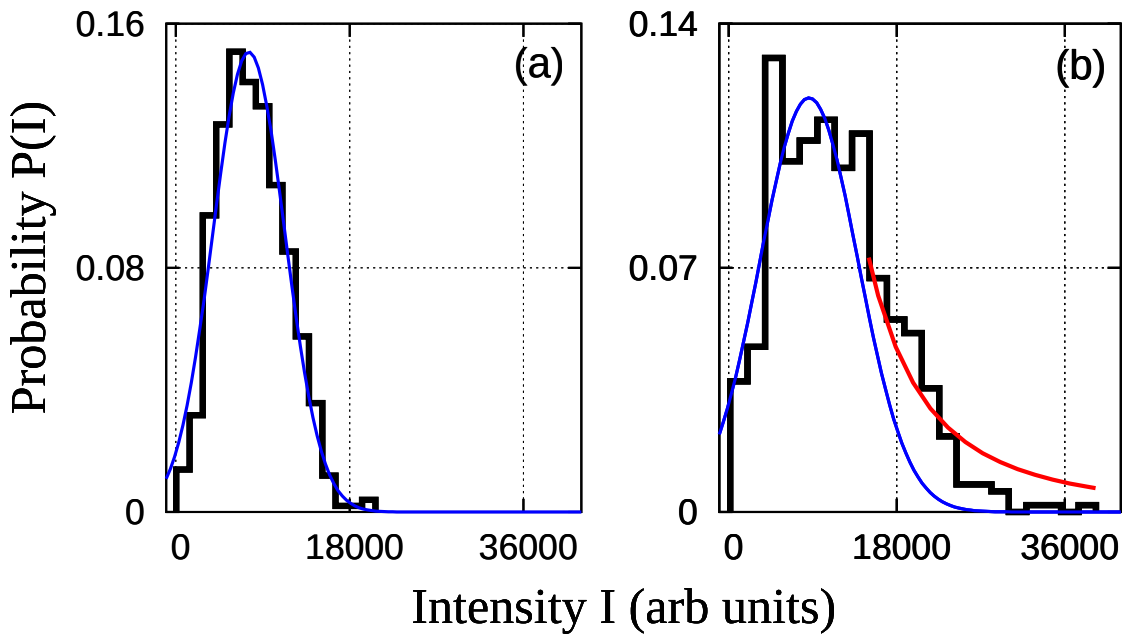

Figure 2.10: *Histograms for R6G (5×10^{-3} M) dye in ethanol (pump energy ~ 3 mJ) containing (a) polystyrene microspheres (size = 0.30 μm, density ~6.3×10^{11}/cc), showing Gaussian statistics (b) TiO_2 microspheres (size = 0.36 μm, density ~ 2×10^{10}/cc), showing Lévy statistics (α = 1.46). Blue and red curves show the Gaussian and the power-law fits, respectively, to the intensity histograms.*

spikes). The two histograms of Fig. 2.12 can be readily understood as corresponding respectively to low and high gain cases. Clearly, at high pump energies for which the corresponding emission intensities are high, the histogram deviates from Gaussian and shows a fat tail. A power-law fit ($g^{-(1+\alpha)}$) to the tail gives a Lévy exponent α of 1.13 (< 2).

Next, we constructed the intensity histograms as function of pump energy for the same system at a lower dye concentration of 5×10^{-3} M (Fig. 2.13). For this case we find that both the intensity histograms at (a) sub-threshold (~ 90 μJ) and (b) above threshold (~ 3 mJ) pumping, display Gaussian statistics. It is, thus, obvious that high gain (or low l_g) required to observe Lévy statistics, could be achieved in our RAMs by increasing both the dye concentration and the pumping. Thus, while at above threshold pumping, the RAM with a dye concentration of 10^{-2} M exhibited Lévy statistics, the RAM with a lower dye concentration of 5×10^{-3} M did not have sufficient gain (l_g^{-1}) – hence, the Gaussian statistics.

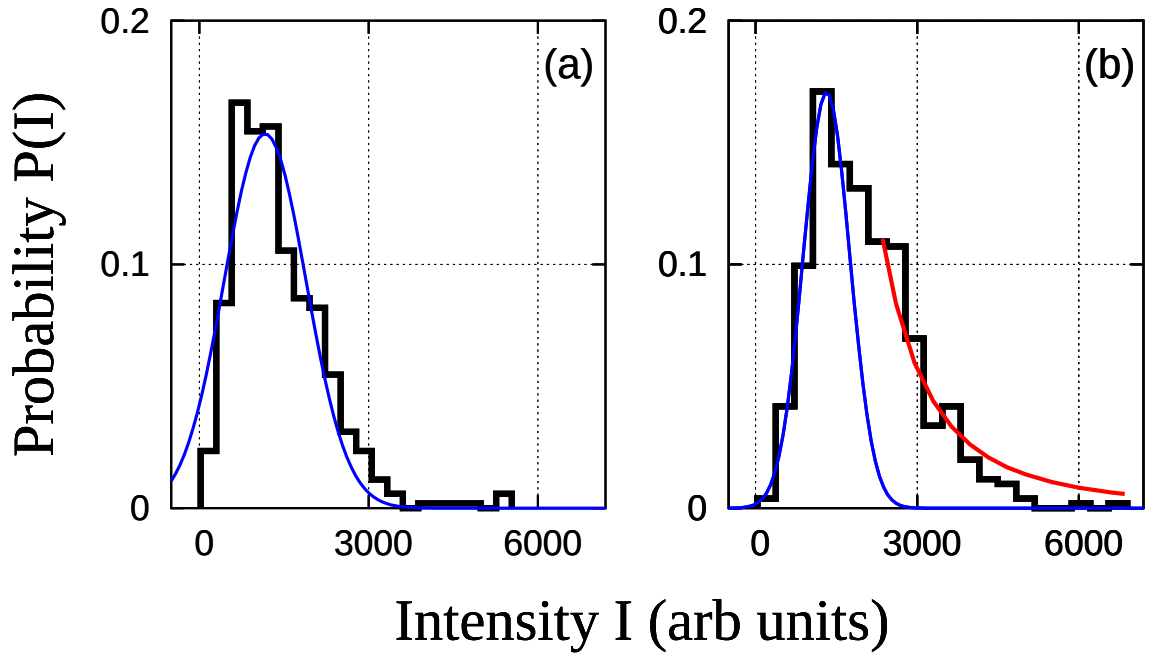

Figure 2.11: *Histograms for R640 perchlorate (10^{-2} M) dye in ethanol (pump energy ~ 3 mJ) containing (a) polystyrene microspheres (size = 0.30 μm, density ~ 6.3×10^{11}/cc), showing Gaussian statistics (b) TiO_2 microspheres (size = 0.36 μm, density ~ 10^{10}/cc), showing Lévy statistics (α = 1.76). Blue and red curves show the Gaussian and the power-law fits, respectively, to the intensity histograms.*

Figures 2.14(a,b) give the intensity histograms for R640 perchlorate(10^{-2} M)-TiO_2 system at (a) sub-threshold pumping of ~ 90 μJ and (b) above threshold pumping of 3 mJ. The intensity statistics is Gaussian for (a) but exhibits Lévy statistics (α = 1.76) for (b). Further, the more pronounced Lévy features observed with R6G dye system as compared to that in R640 perchlorate system, clearly prove the higher quantum efficiency of R6G.

We expect to observe a similar crossover by increasing the dye concentration which effectively reduces the gain length (l_g) and hence the Lévy exponent (α). Figure 2.15(a) gives the histogram for R6G-TiO_2 system (scatterer density ~ $10^{10}/cc$, pump energy ~ 3 mJ) with dye concentration of 5 $\times 10^{-3}$ M. Evidently, the histogram exhibits Gaussian statistics. Figure 2.15(b) shows the histogram when the dye concentration is increased to 10^{-2} M (with all the other RAM parameters like pump energy, scatterer type and density kept the same).

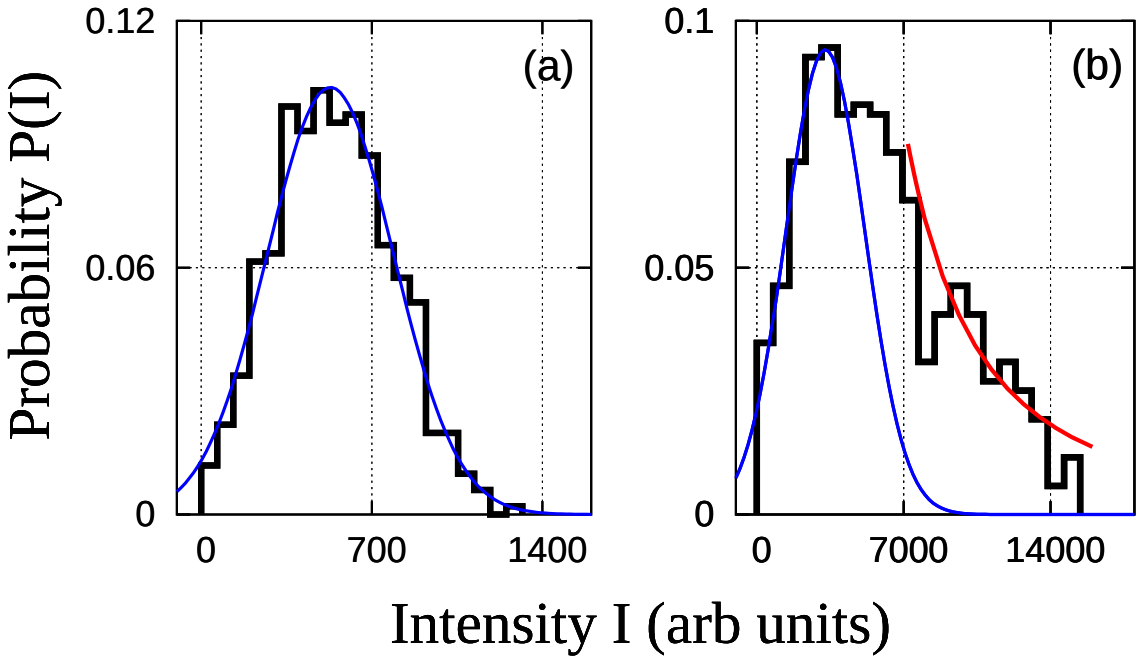

Figure 2.12: *Histograms for R6G (10^{-2} M) in ethanol containing TiO_2 microspheres (scatterer size = 0.36 μm, density ~ 10^{10}/cc), at pump enrgy of (a) ~ 90 μJ, showing Gaussian statistics (b) ~ 3 mJ, showing Lévy statistics (α = 1.13). Blue and red curves show the Gaussian and the power-law fits, respectively, to the intensity histograms.*

Clearly, the statistics is Lévy with Lévy exponent α of 1.13 (< 2).

The effect of increasing the dye concentration was also investigated for the same R6G-TiO_2 system at a higher scatterer density of 2×10^{10}/cc. Fig. 2.16(a) shows the intensity histogram for the R6G(5×10^{-3} M)-TiO_2 system at the scatterer density of 2×10^{10}/cc. Clearly, it exhibits Lévy statistical features with a Lévy exponent (α) of 1.46. Further, the same R6G-TiO_2 system at a higher dye concentration of 10^{-2} M shows more pronounced Lévy features (Fig. 2.16(b)), reflected by a smaller Lévy exponent (α = 0.94). Clearly, while the increase in dye concentration (which is equivalent to increasing the gain within the system) shows a crossover from the Gaussian to the Lévy statistics, an increased scatterer concentration helps reduce the value of the Lévy exponent (α) further, resulting in more pronounced Lévy features.

The crossover as a function of dye concentration was now examined for R640 perchlorate

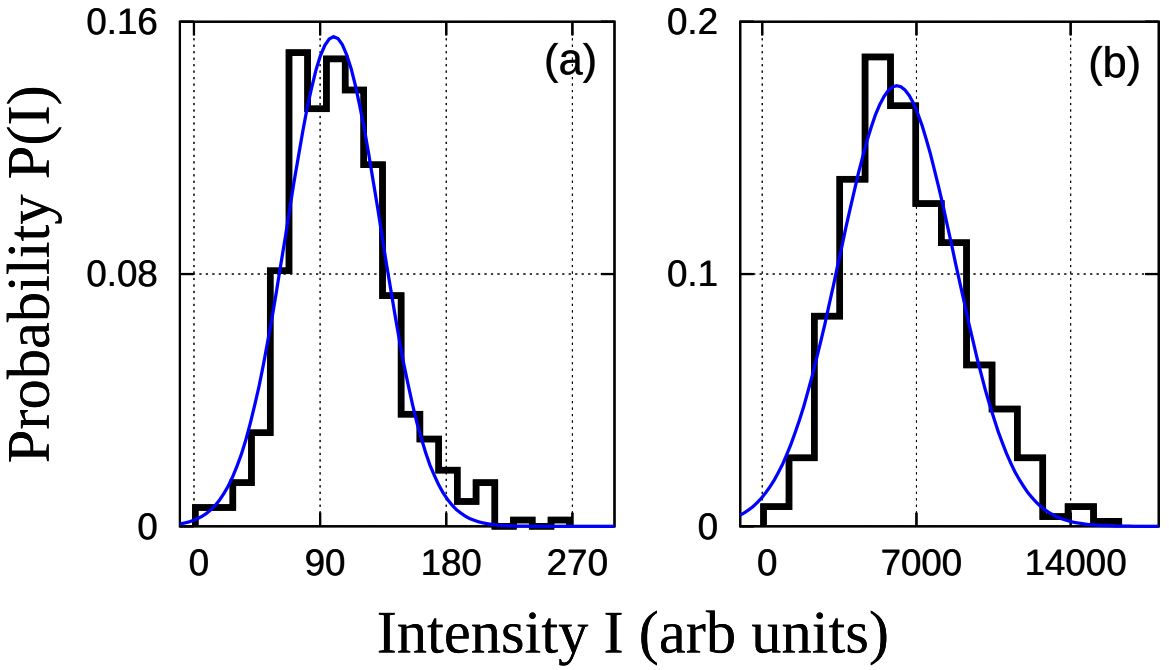

Figure 2.13: *Histograms for R6G (5 $\times 10^{-3}$ M) in ethanol containing TiO_2 microspheres (size = 0.36 μm, density ~ 10^{10}/cc), at pump enrgy of (a) ~ 90 μJ, showing Gaussian statistics (b) ~ 3 mJ, showing Gaussian statistics. Blue curves show the Gaussian fits to the intensity histograms.*

dye. Figures 2.17(a,b) show the intensity histograms for R640 perchlorate-TiO_2 system at dye concentrations of (a) 5×10^{-3} M, and (b) 10^{-2} M. The higher dye concentration which corresponds to higher gain in the system (or low l_g) shows Lévy statistics with exponent (α) 1.46. The statistics is Gaussian for (a). Comparison of Figures 2.15 and 2.17 shows higher quantum efficiency of R6G dye (indicated by lower Lévy exponent α) than that of R640 perchlorate dye.

Thus, we could experimentally demonstrate crossover from the Gaussian to the Lévy statistics by two different ways (namely, the dye concentration and the pumping), both of which alter the gain (l_g^{-1}) in the RAM.

Here we remark that while the pure dye (R6G and R640 perchlorate) samples studied by us showed gain narrowing (FWHM ~ 5 nm), neither narrow emission spikes nor Lévy statistical fluctuations were observed.

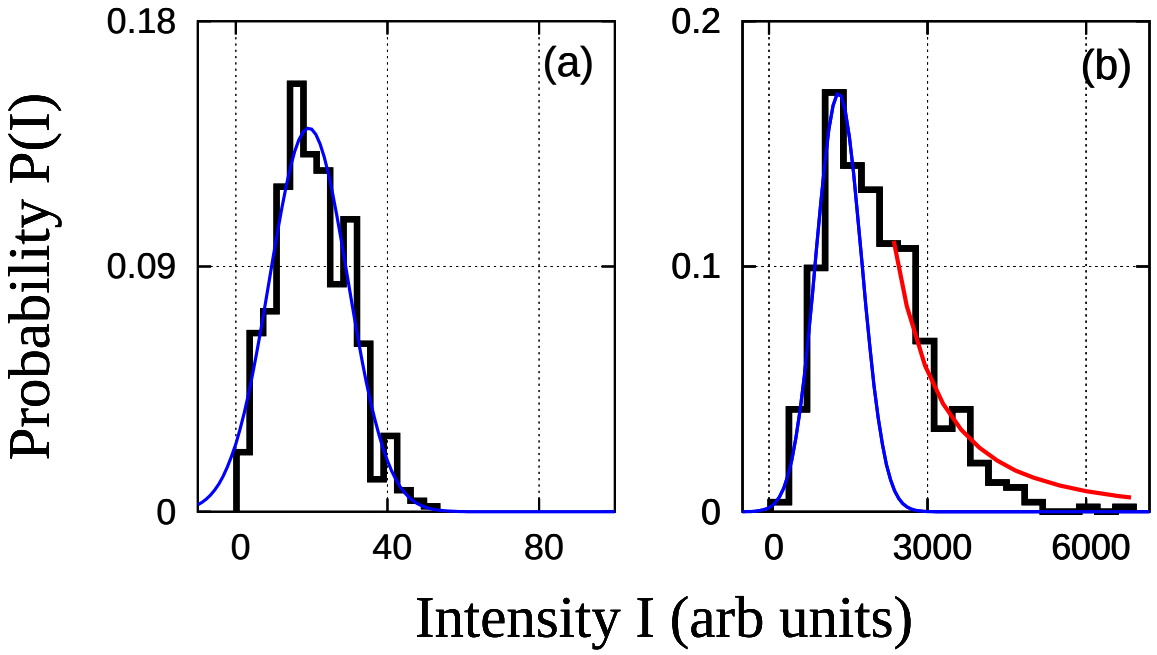

Figure 2.14: *Histograms for R640 perchlorate (10^{-2} M) in ethanol containing TiO_2 microspheres (size = 0.36 μm, density ~ 10^{10}/cc), at pump energy of (a) ~ 90 μJ, showing Gaussian statistics (b) ~ 3 mJ, showing Lévy statistics (α = 1.76). Blue and red curves show the Gaussian and the power-law fits, respectively, to the intensity histograms.*

2.5 Physical interpretation of the experimental results

Due to random multiple scattering, the photons perform a diffusive motion within a RAM. One may think of individual photons performing random walks, leading to a distribution of path lengths. The occurrence of Lévy statistics in the dye-scatterer systems can be understood physically in terms of the distribution of these path lengths of photons in the gain medium. More explicitly, in RAMs, different spontaneously emitted photons follow different paths, and as amplification increases, different photons experience different gains. When scattering is weak, photons have more or less similar path lengths, and thus undergo similar low amplification. However, in the case of very dense scattering media, some of the photons undergo very many scatterings, so that their cumulative path lengths within the bulk medium is extremely long. The gain in the system makes the associated amplification considerable, and these photons then dominate the emission, leading to enhanced intensity whenever such

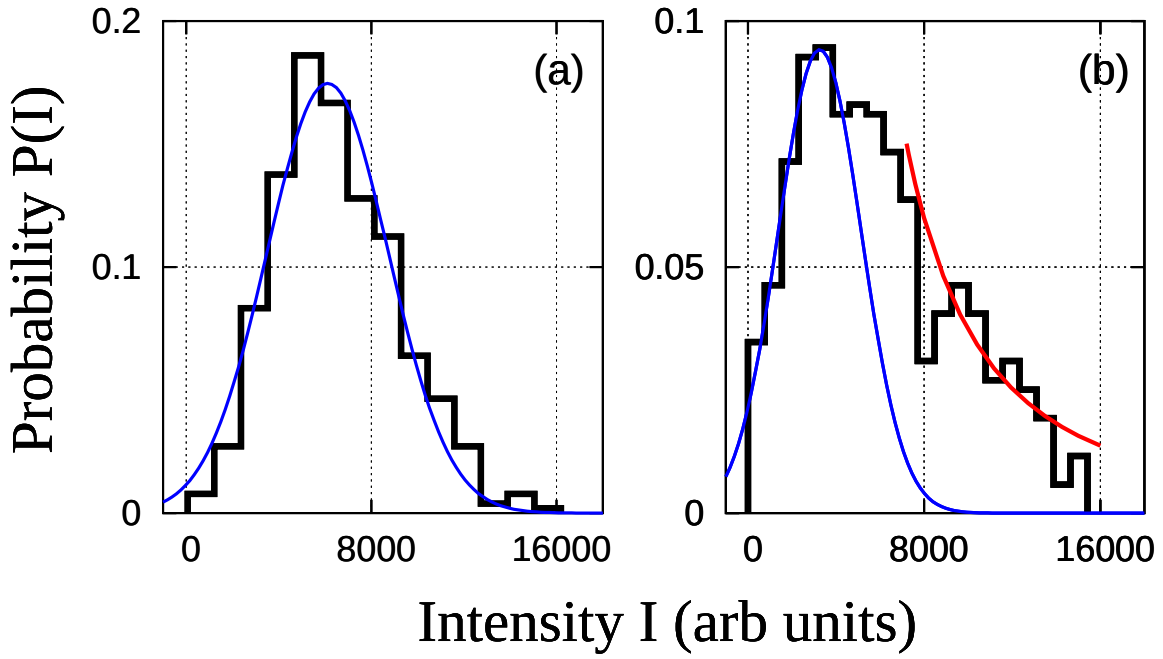

Figure 2.15: *Histograms for R6G-TiO_2 system (size = 0.36 μm, density ~ 10^{10}/cc, pump energy ~ 3 mJ) with dye concentration (a) 5×10^{-3} M, showing Gaussian statistics (b) 10^{-2} M, showing Lévy statistics (α = 1.13). Blue and red curves show the Gaussian and the power-law fits, respectively, to the intensity histograms.*

long paths occur. However, it is to be noted that, their occurrence is rare, and is noticeable only in systems with strong scattering or high gain.

2.6 Conclusions

In conclusion, we have shown theoretically that the emission intensity fluctuations from a random amplifying medium can exhibit Gaussian or Lévy statistics, depending on the scattering (l_t) and the gain (l_g) parameters. A transition from one regime to the other may be brought about, and the Lévy exponent tuned, by altering these two parameters. We have experimentally demonstrated this in dye-scatterer RAMs by four different means, two of which alter the gain characteristics and the other two the scattering strength.

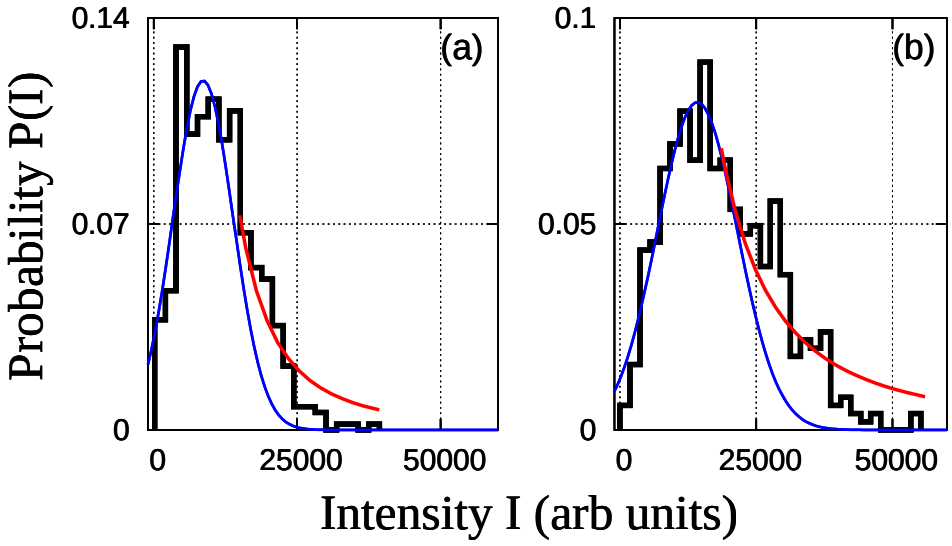

Figure 2.16: *Histograms for R6G-TiO_2 system (size = 0.36 μm, density 2× 10^{10}/cc, pump energy ~ 3 mJ) with dye concentration (a) 5 × 10^{-3} M, showing Lévy statistics (α = 1.46) (b) 10^{-2} M, showing Lévy statistics (α = 0.94). Blue and red curves show the Gaussian and the power-law fits, respectively, to the intensity histograms.*

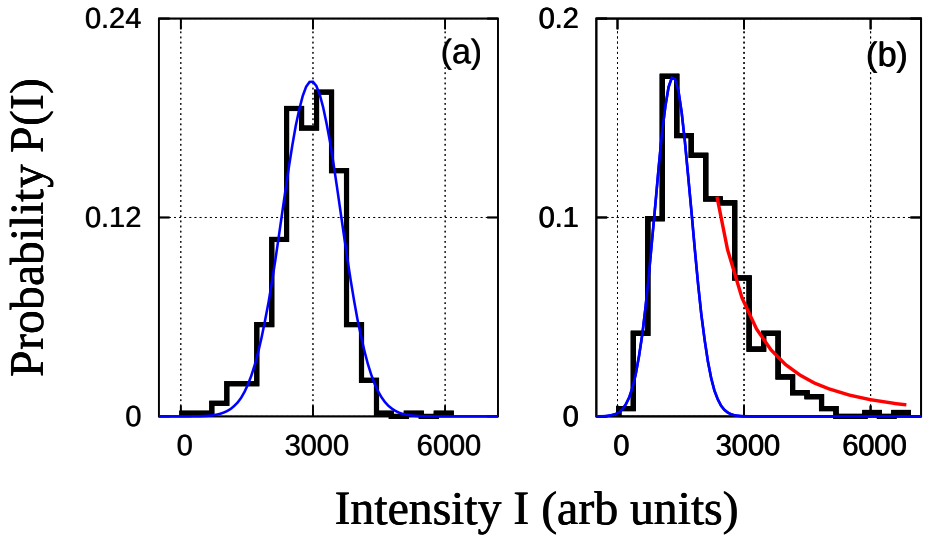

Figure 2.17: *Histograms for R640 perchlorate-TiO_2 system (size = 0.36 μm, density ~ 10^{10}/cc, pump energy ~ 3 mJ) with dye concentration (a) 5 × 10^{-3} M, showing Gaussian statistics (b) 10^{-2} M, showing Lévy statistics (α = 1.46). Blue and red curves show the Gaussian and the power-law fits, respectively, to the intensity histograms.*

Bibliography

[1] see, e.g., P.A. Mello and N. Kumar, *Quantum transport in mesoscopic systems : Complexity and statistical fluctuations*, Oxford University Press (London,2004); Note that the non-selfaveraging is usually invoked in the context of wave-scattering in, and transmission through a random medium where it is due to wave interference. In the present context of classical diffusion, non-selfaveraging of emission arises from the high gain of the random amplifying medium that accentuates the effect of the rare long paths.

[2] G. Zacharakis, N.A. Papadogiannis, G. Filippidis and T.G. Papazoglou, Opt. Lett **25**, 923 (2000).

[3] V.S. Letokhov, Sov. Phy. JETP **26**, 835-840 (1968).

[4] H. Cao, Y.G. Zhao, S.T. Ho, E.W. Seelig, Q.H. Wang and R.P.H. Chang, Phys. Rev. Lett. **82**, 2278 (1999).

[5] H. Cao, J.Y. Xu, S.-H. Chang and S.T. Ho, Phys. Rev. E **61**, 1985 (2000).

[6] S. Mujumdar, M. Ricci, R. Torre and D.S. Wiersma, Phys. Rev. Lett. **93**, 053903 (2004).